Study of self-limiting oxidation of silicon nanoclusters by atomistic simulations

J. Dalla Torre,[a] J.-L. Bocquet, Y. Limoge, J.-P. Crocombette, E. Adam, and G. Martin
Commissariat à l'Énergie Atomique–CEA Saclay, Service de Recherche de Métallurgie Physique, 91191 Gif-sur-Yvette Cedex, France

T. Baron
Laboratoire des Technologies de la Micro-électronique, CNRS, Grenoble, France

P. Rivallin and P. Mur
CEA-DRT, LETI/DTS, CEA/GRE, 17, Avenue des Martyrs, 38 054 Grenoble Cedex 9, France

(Received 1 April 2002; accepted for publication 3 May 2002)

We present molecular dynamics simulations directed at understanding self-limiting oxidation of nanoclusters. Atomic oxygen is inserted in an atom-by-atom way in the silicon bonds to form silicon oxide. First, we focus on planar oxidation to calibrate our model and test its capabilities. Then, we present results on oxidation of 50 Å diam silicon spheres. Kinetic causes of self-limitation are investigated by drawing a map of the local stress in the Si/SiO_2 system. We obtain stresses in contrast to in continuum models. For thin oxides, we find in particular tensile pressure in the silicon core and a pressure gradient in the oxide shell. We investigate the effect of pressure gradient on the O_2 transport within the framework of Nerst–Eintein's transport equation. We find that a pressure gradient compatible with experimental estimates yields self-limitation of the oxidation kinetics.
© *2002 American Institute of Physics.* [DOI: 10.1063/1.1489094]

I. INTRODUCTION

The oxidation kinetics of a non planar silicon surface were already of great interest to the microelectrics industry in the 1980s.[1] It was observed that oxide growth on a curved surface was retarded. This retardation was observed to depend on the growth temperature, the radius of curvature and the sign of curvature (convex or concave shape) that leads to inhomogeneity of the oxide thickness at corners. This effect was of concern for the design of, e.g., metal–oxide–semiconductor (MOS) devices.

The oxidation rate decreases with downsizing[1–3] and this effect is greatly enhanced and exhibits self-limiting behavior at the nanometer scale. More recently, the idea of taking advantage of the self-limiting oxidation of nanoclusters (either nanoislands[2] or nanospheres[3]) and of nanowires[4,5] was proposed to monitor the size and the size distribution of an assembly of nanometer objects. Monitoring the characteristics of such nanostructures is of interest for future opto- and microelectronics devices like, e.g., quantum dot based single electron devices.[6]

Self-limiting oxidation of cylinders has been studied first and is related to the particular stress that develops in nonplanar oxidation.[1,7,8] In the absence of stress, the oxide growth rate of convex structures should be larger than planar oxidation because of greater exposure to the ambient[1,2] (or tip effect). Liu and co-workers[5] mentioned the idea that the oxidation kinetic pathway may lead to a deep metastable equilibrium state. They concluded that constrained equilibrium was unlikely because of the highly exothermic nature of the oxidation reaction.

Usually, it is believed that self-limitation arises from kinetic processes, i.e., the stress-dependent oxidation reaction rate or oxidant transport in the SiO_2. Continuum models based on the former were developed to predict the growth evolution of the oxide. A continuum stress model was coupled to a diffusion-reaction equation[9] to describe the time evolution of the oxide front.[1,10] Stress was assumed to affect the oxidant reaction rate (K), oxidant diffusion (D) and/or oxidant solubility at the SiO_2 surface (c^*) in the following way:[1,10]

$$K = K_0 \exp\left(\frac{\sigma_{rr} v_K}{k_B T}\right), \tag{1}$$

$$D = D_0 \exp\left(-\frac{p v_D}{k_B T}\right), \tag{2}$$

$$c^* = c_0^* \exp\left(-\frac{p v_c}{k_B T}\right), \tag{3}$$

where the subscript 0 indicates the stress free value, k_B is the Boltzmann constant, T the temperature, p the hydrostatic pressure, σ_{rr} the normal stress in the silicon at the Si/SiO_2 interface, and v_K, v_D and v_c are activation volumes. $\sigma_{rr} < 0$ and $p > 0$ correspond to compressive stresses in the present sign convention. A compressive (tensile) σ_{rr} in the silicon core would slow down (speed up) the reaction rate. A compressive (tensile) pressure in the SiO_2 would reduce (increase) the oxidant diffusion and concentration.

Several models of the SiO_2 mechanical behavior have been suggested to serve as stress input for K, D and c^*. SiO_2 is considered an elastic solid, viscous fluid or viscoelastic liquid or solid (see, e.g., Ref. 10 and references therein). It is

[a]Electronic mail: jdallatorre@cea.fr

 © 2002 American Institute of Physics

Downloaded 02 Jul 2002 to 132.166.68.80. Redistribution subject to AIP license or copyright, see http://ojps.aip.org/japo/japcr.jsp

proposed that for temperature below the oxide flow (<950 °C) the lower growth rate observed on, e.g., convex surfaces is the result of isotropic compressive stress (consequently compressive pressure) that builds up in the silicon core and slows down the reaction rate.[1] These models were very successful at predicting oxide growth evolution at the micrometer scale. This modeling was extended to nanometer scale features. Chen and co-worker showed that it is possible to reproduce self-limiting oxidation behavior of silicon nanowires[11] and nanoislands.[12]

On the experimental side, several discrepancies with respect to the classical models were observed in nanometer features. First, Liu *et al.*[5] observed dependence of the limiting core diameter of silicon cylinders on the oxide thickness. This suggests oxidant diffusion as an explanation of the self-limiting oxidation of their nanowires. Recently, Delph's modeling[8] suggested that the existence of a boundary layer in which stress varies drastically may affect oxidant diffusion. Next, Hofmeister *et al.*[3] showed that the oxidation of nanospheres also presents unusual behavior. Small oxidized particles (<5 nm) indicate near zero or even tensile stress in their silicon core. They expected the state of the cluster to correspond to the saturation configuration.

Modeling at the atomic scale seems to be well suited for studying these systems. However, limitations still come from the size of the system (few tens of nanometers) and the oxidation time scale (ranging from minutes to hours). *Ab initio* calculations (static or molecular dynamics) have proven very useful in studying elementary atomistic mechanisms of silicon oxidation (see, e.g., Chaps. 6, 7 and 10 of Ref. 13 and references therein) but are restricted to systems of a few hundred atoms. Kinetic Monte Carlo methods are promising methods that allow one to study the length and time scales comparable to those in experiments.[14] However, this technique requires prior knowledge of the elementary oxidation reaction processes. This method neither tackles stress nor strain as atomic positions are generally restricted to some fixed lattice sites even if some progress has been made to cope with "soft lattice models."[15,16] Equilibrium Monte Carlo techniques coupled to an interatomic potential that allow continuous variations of the atomic position have been used to simulate the structure of the Si/SiO_2 interface.[17,18] These simulations allow one to extract some information on the stress distribution of equilibrium structures but they may miss features that result from the kinetics of the oxidation.

An intermediate approach between first principle calculations and Monte Carlo was proposed by Watanabe and Ohdomari based on molecular dynamics (MD).[19] They used an extended Stillinger–Weber potential developed for Si/O mixed systems.[20] This empirical potential is well suited for the study of large systems and for extracting local stresses. Schematic construction of the oxide is carried out: oxygen atoms are directly inserted into the Si–Si bonds in a layer-by-layer way and a molecular dynamics technique is used to relax the structure obtained. We chose a similar approach to investigate stress development during oxidation of silicon nanospheres. In our method the oxygen is inserted atom by atom into the silicon structure. This approach does not deal with the particular oxidation mechanisms that correspond to different oxidant species (O_2, H_2O, or O). There are differences in the oxidation for, e.g., molecular or atomic oxygen.[21] The defect population produced at the interface or in the oxide by particular oxidant species affects the mechanical properties.[22] We propose that the mechanical behavior presented in this work is generic. The model is presented in Sec. II. Since planar oxidation has been widely studied experimentally, we use this system to assess the capabilities and limitations of our modeling procedure. Next, we apply this procedure to the oxidation of silicon nanospheres. We discuss the constrained equilibrium hypothesis and we assess kinetic effects by computing local stresses in the sphere. Our results are discussed and an analytical model is proposed to illustrate the importance of stress on oxidant transport.

II. SIMULATION TECHNIQUE

In order to describe the oxidation of silicon substrates, we use standard constant temperature MD simulations with a Stillinger–Weber like potential extended by Watanabe *et al.*[20] to treat Si/O mixed systems. The velocities of the particles are scaled to obtain the average temperature required[23] and we use a simple Verlet algorithm to solve Newton's equations with a time step of $\delta t = 10^{-16}$ s.

The potential consists of two-body and three-body interactions. The two-body term includes interactions between Si–Si and Si–O pairs, whereas the O–O interaction is considered purely repulsive. Consequently, the O–O bonding cannot be considered. The three-body term includes triplets with combinations of Si and O, excluding O–O–Si and O–O–O terms. The potential function can treat the Si/SiO_2 interface where Si, SiO_2 and SiO_x ($x<2$) suboxides are present. We use the parameters given in the original paper which were based on first principle calculations. The simplicity and the short cutoff distances of the potential allow one to perform a large number of MD steps.

The oxide formation procedure is important in order to produce a kinetic pathway that is as realistic as possible. Starting from a silicon bare flat substrate or sphere, the oxide is formed by introducting the oxygen, atom by atom, directly into the Si–Si bonds.

The insertion procedure follows some basic rules that are illustrated in Fig. 1 and that are summarized here.

To initiate the oxidation we start with the bare silicon substrate. A few oxygen atoms are inserted at randomly selected Si dangling bonds on the silicon surface (1%–10% of the dangling bonds are occupied by oxygen). These oxygens atoms make up the initial nuclei for subsequent oxidation in steps (i)–(iii) (Fig. 1).

(i) We want to insert a new oxygen atom into one of the Si–Si bonds in the system (dangling bonds can no longer be chosen). We select a Si atom provided it is bound to at least one and at most three oxygen atoms. The first candidates are therefore the silicon atoms selected from the initial nucleation process or from the interface atoms in later oxidation (Fig. 1).

(ii) Many Si atoms may be selected according to step (i). We chose the Si atom with the highest z coordinate

Downloaded 02 Jul 2002 to 132.166.68.80. Redistribution subject to AIP license or copyright, see http://ojps.aip.org/japo/japcr.jsp

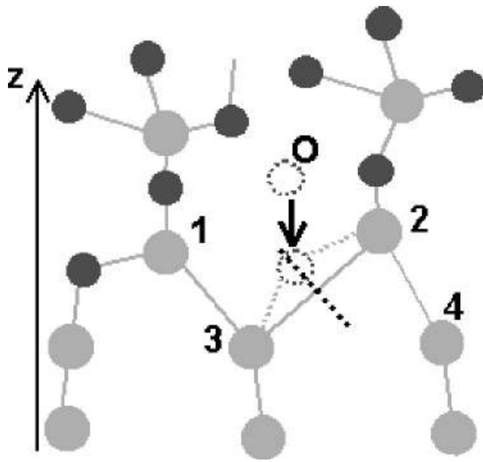

FIG. 1. Schematics of a Si/SiO_2 interface in planar oxidation. The light gray atoms correspond to silicon and the dark gray to oxygen atoms. The dashed circles represent the oxygen to be inserted. Following rule (i), atoms 1 and 2 are bound to at least one and at most three oxygens. Atom 2 corresponds to the atom with the highest position or z coordinate [rule (ii)]. The oxygen may either be inserted into the Si(2)–Si(3) or the Si(2)–Si(4) bond. The longest bond [Si(2)–Si(3)] is selected from rule (iii). Finally, the oxygen is inserted at a position which complies with the Si–O bond length.

along the normal to the free surface in the case of a planar substrate (Fig. 1). The largest distance to the center is used for sphere oxidation.

(iii) While a Si atom is selected, several bonds to neighboring Si atoms can be candidates for O insertion. We chose the longest bond. Since the Si–Si distance increases from about 2.35 Å in silicon to about 3 Å in amorphous SiO_2, we expect the cost in strain energy to be lower for a stretched bond, in accordance to the general expectation that the oxidation reaction barrier would be lower.[1]

Insertion steps (i)–(iii) can be repeated p times, every n MD step. p and n fix the "growth rate" of the oxide for a given substrate size. Typically, a single atom ($p=1$) is inserted every 100 δt ($n=100$).

Rules (i) and (ii) force the oxide to grow layer by layer. This is observed experimentally in planar oxidation (see, e.g., Chaps. 3 and 5 in Ref. 13). We assume layer-by-layer growth in the oxidation of spheres because no clear roughening of the Si/SiO_2 is seen in electron microscopy images.[3]

Note that placing the oxygen atom in the middle of the Si–Si bond in rule (iii) can yield some thermal spiking at the interface. In this position the Si–O bond length is still shorter (~1.2 Å) than the expected Si–O bond length (~1.6 Å) and the extra potential energy is quickly released and produces a large thermal spike. Our thermostat procedure regulates the overall temperature of the system and is not efficient in releasing this energy locally. We circumvent this problem by placing the oxygen atom in a random direction of the midplane of the Si–Si bond in such a way as to satisfy the 1.6 Å Si–O bond length (Fig. 1). Heating is not completely avoided (constraints on triplet bond angles are not satisfied). A specific thermostat is applied to the atoms that have kinetic energy that corresponds to an instantaneous temperature larger than 2000 K. The kinetic energy of each atom is checked every 10 δt.

III. RESULTS FOR PLANAR OXIDATION

Here, we apply our model to planar oxidation to assess its domain of validity. A silicon diamond crystal structure is first built; it is terminated by a (001) (z-axis) surface and x and y axes aligned in the $\langle 110 \rangle$ directions. We force (2×1) dimer reconstruction and the crystal is free to relax in the [001] direction. The silicon substrate consists of 14×14 atoms per atomic layer and is 48 atomic layers high. A constant temperature of 1200 K is set in the simulation cell. This corresponds to a temperature below the oxide flow temperature at the experimental time scale. The silicon substrate is forced to match a lattice parameter thanks to periodic boundary conditions applied in the horizontal directions. Doing so, we simulate the fact that the wafer substrate is thicker than the oxide layer.

To quantify the growth rate in the simulations, we introduce the notion of an oxygen monolayer (ML) inserted into the silicon structure. {001} silicon planes are constituted of 196 atoms. Oxidation of 1 ML proceeds by introducing 392 oxygen atoms that correspond to the 392 Si–Si bonds between two successive {001} planes. Ideally, complete insertion of the 392 O would lead to the formation of a new stoichiometric SiO_2 layer (upper plane) and of a SiO suboxide layer (lower plane) (this is correct for all layers except the first one because of the initial nucleation step of our oxidation method). For the sake of simplicity, we consider that oxidation of 1 ML corresponds to the insertion of one oxygen monolayer (392 O) or to the formation of one SiO_2 monolayer.

The oxygen insertion follows the scheme described in Sec. II. Five oxygen atoms are inserted periodically at the Si/SiO_2 every 100 δt. 8500 oxygen atoms are inserted into the silicon structure presented in Fig. 2(a). This corresponds roughly to the growth of a 21.7 (oxide) ML.

We compute the local stress tensor that develops in the structure in Fig. 2 as follows. The instantaneous stress tensor in a volume Ω is defined following the general expression:

$$\sigma^{\alpha\beta}=\frac{1}{\Omega}\frac{\partial E}{\partial e^{\alpha\beta}}. \tag{4}$$

E is the total energy of the N particles in volume Ω and $e^{\alpha\beta}$ is a component of the strain tensor. Considering a system with periodic boundary conditions, the atoms in volume Ω can interact with the atoms in the image cells. E is a simple function of $(\mathbf{p_1},\ldots,\mathbf{p_N};\mathbf{r_1},\ldots,\mathbf{r_N})$, and $\mathbf{p_i}$ and $\mathbf{r_i}$ are the momentum and the position vectors of the ith particle. The instantaneous stress tensor is given by[24,25]

$$\sigma^{\alpha\beta}=-\frac{1}{\Omega}\left(\sum_{i=1}^{N}\frac{p_i^{\alpha}p_i^{\beta}}{m_i}-\sum_{i=1}^{N}r_i^{\beta}\frac{dV}{dr_i^{\alpha}}\right), \tag{5}$$

in which the superscript α or β points to component α or β of position $\mathbf{r_i}$ and momentum $\mathbf{p_i}$ of the ith particle, with mass m_i. V is the potential energy part of E. The derivatives of V are determined from the expression of the interatomic potential.

Downloaded 02 Jul 2002 to 132.166.68.80. Redistribution subject to AIP license or copyright, see http://ojps.aip.org/japo/japcr.jsp

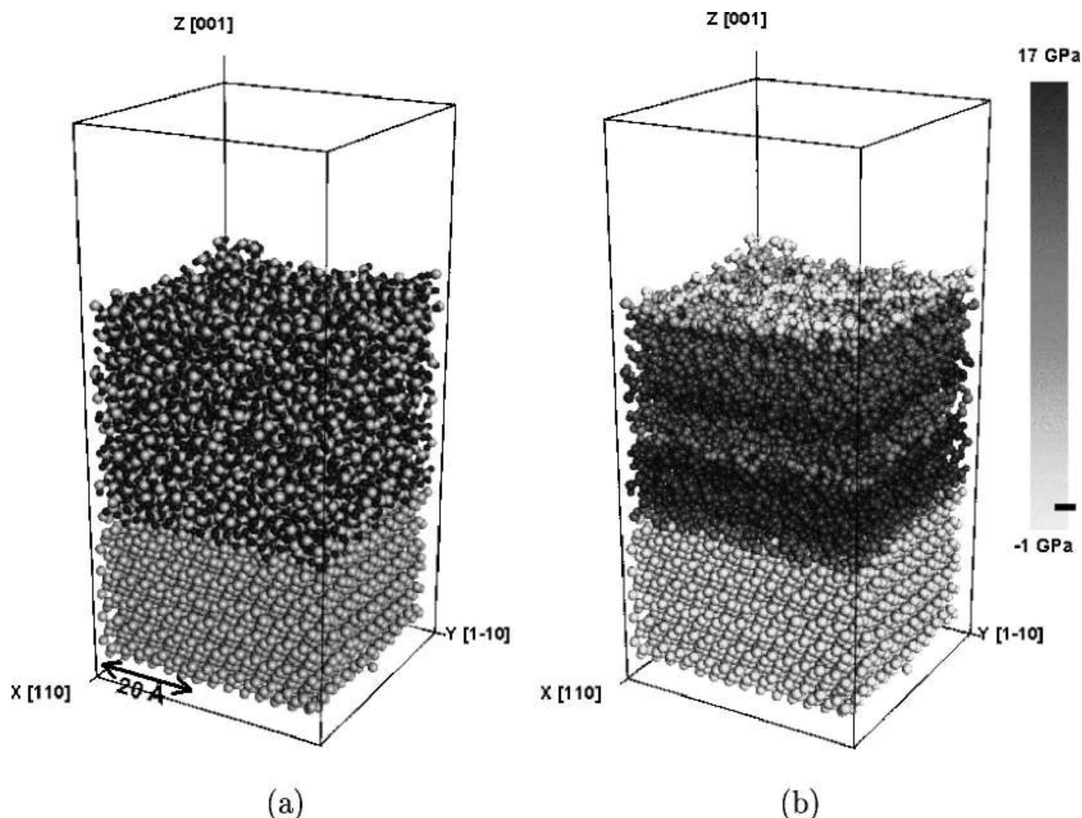

FIG. 2. (a) Morphology of the oxidized silicon substrate after insertion of 8500 oxygen atoms at a temperature of $T=1200$ K and an oxide growth rate of $F=1.25$ ML/ps. Light gray and dark gray spheres correspond, respectively, to Si and O atoms. (b) Pressure map through the Si/SiO_2 structure. The layer is divided into 3 Å thick slices and the pressure in each slice is computed. The gray scale corresponds to the pressure value and the same pressure is attributed to the atoms that belong to the same slice.

If one wishes to compute the local stress in a finite volume containing N particles that is part of a larger system, the atoms in this volume interact with N_{ext} external particles. The energy of interaction has to be shared between the internal and the external particles. E is now a function of the N and N_{ext} particle positions, $(\mathbf{p_1},\ldots,\mathbf{p_N};\ \mathbf{r_1},\ldots,\mathbf{r_N};\ \mathbf{r_N}+\mathbf{1},\ldots,\mathbf{r_N}+\mathbf{N_{ext}})$ and expression (5) becomes

$$\sigma^{\alpha\beta}=-\frac{1}{\Omega}\left(\sum_{i=1}^{N}\frac{p_i^{\alpha}p_i^{\beta}}{m_i}-\sum_{i=1}^{N+N_{\mathrm{ext}}}r_i^{\beta}\frac{dV}{dr_i^{\alpha}}\right). \qquad (6)$$

In order to compute the local stress with reasonable statistical fluctuations, we defined equal volumes Ω by dividing the system into 3 Å thick slices along the z axis. We start from the lowest atom in the simulation cell.

The instantaneous stress components of the stress tensor $\bar{\bar{\sigma}}$ at the end of the simulation were computed as was the pressure p defined as $p=-\frac{1}{3}\mathrm{Tr}\,\bar{\bar{\sigma}}$. The pressure results are presented in Figs. 2(b) and 3.

By comparing Figs. 2(a) and 2(b), we see the oxide layer corresponds to a highly compressive pressure $(p>0)$ zone. In the oxide slices, the stress tensor has the form

$$\bar{\bar{\sigma}}\begin{pmatrix}\sigma & 0 & 0\\ 0 & \sigma & 0\\ 0 & 0 & 0\end{pmatrix}. \qquad (7)$$

What we have considered as zero stress components corresponds to computed stress at least one order of magnitude lower than σ. These can be larger than the accuracy of the stress calculation ($\sim$0.1 GPa).

The pressure in each slice along the z axis is reported in Fig. 3. Compressive pressure in the range of 0–3 GPa is computed in the region that corresponds to the silicon sub-

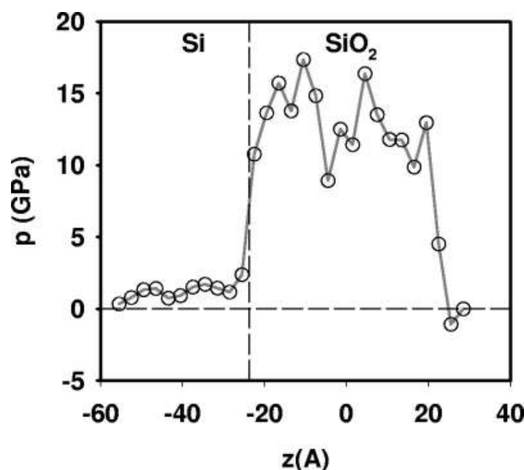

FIG. 3. Pressure in the slices along the z axis. The horizontal dashed line indicates zero pressure while the vertical dashed line identifies the Si/SiO_2 interface.

Downloaded 02 Jul 2002 to 132.166.68.80. Redistribution subject to AIP license or copyright, see http://ojps.aip.org/japo/japcr.jsp

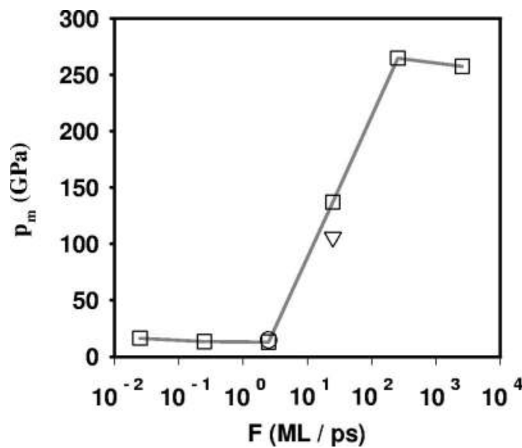

FIG. 4. Maximum pressure in the oxide layer as a function of the oxygen insertion rate. The squares are for $F=0.025$ ML/ps (1 O inserted every $1000\delta t$), 0.25 ML/ps (1 O/$100\delta t$), 2.5 ML/ps (1 O/$10\delta t$), 25 ML/ps (1 O/$1\delta t$), 255 ML/ps (10 O/$1\delta t$), and 2551 ML/ps (100 O/$1\delta t$). The circle corresponds to $F=2.5$ ML/ps (10 O/$100\delta t$) and the inverted triangle to $F=25$ ML/ps (100 O/$100\delta t$).

strate ($z\sim-55$ to -25 Å). The pressure evolves quickly toward higher values as it crosses the interface, fluctuates around a constant value (~13 GPa) in the oxide and finally falls to zero at the free surface.

The lateral dimensions of the cell were chosen in order to obtain the silicon lattice spacing at 0 K. Thus, the stress computed in the silicon substrate results from thermal expansion. This stress is small compared to σ because of the periodic boundary conditions in the horizontal directions that do not allow strain to take place in the substrate far enough from the interface. In the oxide, the compressive stress results from the volume expansion associated with the silicon to oxide reaction (the atomic volume of a Si atom in silicon is 20 Å^3 while the molar volume of a SiO_2 molecule is 45 Å^3). Our simulations are in qualitative agreement with experimental and simulation data. Compressive stress was observed in wet and dry oxides grown on silicon wafers[26,27] and rather uniform strain energy even right up to the interface was found in Monte Carlo atomistic simulations.[17] However, our simulations yield stresses one to two orders of magnitude higher than in the experiments.

We explored different causes of these discrepancies using test structures made up of thinner oxide films (4 ML) and grown under the same conditions. The lateral dimensions of the cell were extended to match a lattice spacing which relaxes the stress resulting from thermal expansion. Oxide was also grown using different substrate sizes ranging from 4×4 atoms to 20×20 atoms; we did not observe any significant difference in the stress level in the oxide.

Finally, we found that the growth rate of the oxide may be important for the resulting stress. In Fig. 4, we plot the maximum pressure within the different slices in the oxide layer. A large deposition rate induces compressive stresses up to several hundred GPa while lower deposition rates reduce them to a few 10 GPa. The deposition rate is not defined in a unique way in our method. To produce $F=25$ ML/ps, we could insert $p=1$ O every $n=1$ δt or $p=100$ O every $n=100$ δt. Only a weak dependence of the result was exhibited for the combination of p and n that we used (see Fig. 4).

The unrealistic stresses for $F>10$ ML/ps result in highly defective interfaces (voids, dangling bonds, etc.) whereas the good quality of the Si/SiO_2 interface is a well documented fact. In the low stress regime, a newly inserted oxygen atom has enough time (~ a few periods of atomic vibration) to relax its position before a new oxygen atom is inserted into its neighborhood. An oxide growth rate as low as 0.025 ML/ps did not produce more stress relaxation. Plastic relaxation processes are not accessible for such high growth rate compared to experimental ones: real oxidations extend from minutes to hours. We tried to activate these processes by increasing the temperature in the simulations. While at 1600 K no effect was observable, higher temperature (2000 K) produced silicon melting. Another limitation of the technique might come from the capability of the potential to reproduce realistically the defects involved in such plastic processes.[28] Note that the simulations presented in Fig. 2 were carried out in the lower deposition rate or stress regime.

To summarize, our modeling technique provides consistent silicon, oxide and interface structures and a qualitative description of stress evolution. The stress evolution and its sign are governed by the system geometry and the volume expansion which results from the formation of oxide.

IV. SPHERE OXIDATION RESULTS

Silicon spheres were constructed from bulk silicon in a square box with periodic boundary conditions. The atom closest to the center of the box was chosen to be the center of the sphere. To build a sphere with radius r_0, atom to center distances were calculated for every atom in the box. The atoms which corresponded to a distance larger than r_0 were deleted from the simulation cell. The initial box size needs to be large enough to avoid interaction of the sphere with its images during the simulation (oxidation causes volume expansion of the system). We constructed a silicon sphere containing 3265 Si atoms corresponding to a 50 Å diam sphere. The size of the system corresponds to experiments and allows extensive calculations on a single processor computer. Molecular dynamics were started at 1200 K and the sphere was free to relax and to reconstruct its surface for $10\,000\delta t$ before starting the oxygen insertion. The oxide was grown by inserting 6000 oxygen atoms and a ~15 Å thick oxide was obtained. One oxygen atom is inserted every $100\delta t$, but it does not correspond to a constant growth rate: the silicon radius decreases over time and the growth rate of the SiO_2 shell increases. However, we saw in Sec. III that stresses do not vary much in our simulations for a wide range of growth rates.

First, we check if our modeling yields, the same conclusion as Liu *et al.*[5] (for nanowire oxidation) concerning the hypothesis of constrained equilibrium for nanosphere oxidation. To do this, we compute an "average" energy gain per oxygen atom inserted using the procedure that follows. We start by defining n_O as the number of oxygen atoms inserted. Since 1 O is inserted every $100\delta t$: $n_O=\text{time}/100\delta t$. Next, the potential energy of the system $V(n_O)$ is computed every $(1/10)n_O$. It presents large fluctuations, e.g., at the insertion

Downloaded 02 Jul 2002 to 132.166.68.80. Redistribution subject to AIP license or copyright, see http://ojps.aip.org/japo/japcr.jsp

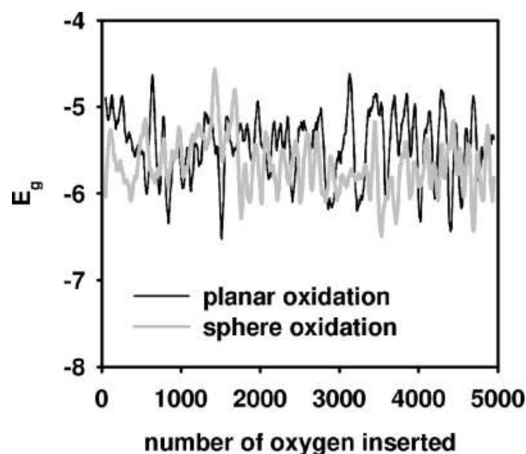

FIG. 5. *Average* potential energy gain per oxygen atom inserted. E_g is plotted for the first 5000 oxygen insertions in planar oxidation and sphere oxidation.

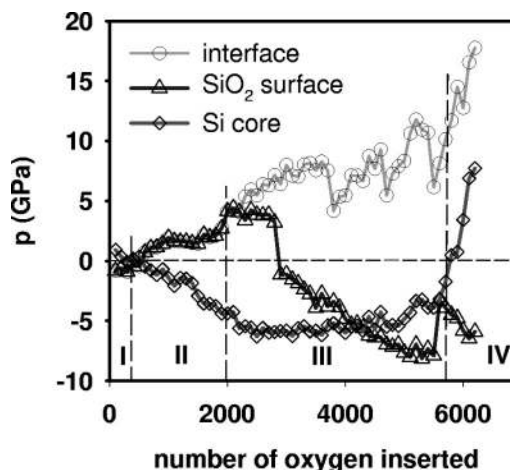

FIG. 6. Pressure calculated in the silicon core, at the oxide interface and at the oxide surface as a function of the number of oxygen atoms inserted. The oxidation sequence is divided into four stages, I–IV.

of a new O that yields a jump of the system potential energy. Each data point is averaged with neighboring data points over an interval corresponding to 100 n_O. The slope of $V(n_O)$ is computed and averaged again over an interval of $10n_O$. This averaged slope is plotted in Fig. 5, and represents an average potential energy gain per oxygen inserted. This procedure was carried out for the flat substrate (from simulation in Fig. 2) and sphere oxidation (Fig. 5). Note that the same number of O atoms inserted does not correspond to the same oxide thickness in the two cases. The flat substrate and sphere plots fluctuate around a common average negative value of E_g. Most important , the sphere does not present any clear evolution with the number of O atoms inserted (i.e., the oxide thickness or time).

Let us assume that the system evolves to an equilibrium state that would stop oxide formation as a result of stress. During oxidation, the potential energy gain per O inserted (E_g) should decrease up to a point where the oxidation reaction $O_2+Si\rightarrow SiO_2$ is reversed. Si–O bonds are strong and O insertion lowers the system's potential energy (E_g is negative). Strain energies resulting from the different stresses that develop in the flat substrate and sphere oxidation are small and do not show significant effect on E_g. As concluded by Liu *et al.*,[5] the energetic balance of oxidation is not appreciably shifted by the stress in our modeling.

To assess kinetic limitations, we compute local stresses in the sphere. We first need to define volumes for the stress calculation. We divide the sphere into 3Å thick shells (the center volume is just a sphere of 3Å radius). With this procedure, volumes are not constant and, e.g., the computed stress in the central sphere is subject to larger fluctuations than in the outside shells. The stress is computed in Cartesian coordinates (x,y,z) and transformed into spherical coordinates (r,θ,φ).

The pressure evolution at different locations in the system (silicon, oxide interface and surface) is presented in Fig. 6 where the curve labeled ''silicon core'' corresponds to the pressure from one of the silicon shells near the interface. The ''interface'' curve corresponds to the oxide shell near the Si/SiO_2 interface. The surface pressure is extracted from the last shell that contains atoms. But because the surface moves during oxidation, the last shell may be poorly filled so we sometimes use the next to last shell. The local pressure calculations are also displayed (Fig. 7) at different stages of the oxidation.

The oxide evolution was divided into four stages in Fig. 6.

In stage I, until a few 100 oxygen atoms have been inserted, we find slight compressive pressure in the silicon core and tensile pressure in the partially oxidized layer.

Stage II extends to about 2000 oxygen atoms being inserted. A continuous SiO_2 shell forms [Figs. 7(a) and (b)]. Clear compressive pressure takes place at the interface in the oxide and the silicon core becomes tensile. Figure 7(b) indicates there is homogeneous pressure in the silicon core.

When the oxide gets thicker (stage III), the pressure at the surface and at the interface of the oxide follow distinct evolutions. The pressure at the interface is compressive and almost constant until ~5500 oxygen atoms are inserted. The surface pressure, on the other hand, evolves from compressive to tensile as the oxide thickens [Fig. 7(c)].

Finally, for an oxide thickness of 15–20 Å (stage IV), a dramatic change comes from the silicon core that goes from a tensile to compressive state [Fig. 7(d)].

Some oscillations are observed in the interface and surface plots in Fig. 6. These are the result of interface and surface motion. The interface shell can include some silicon and the surface shell can include some empty space. Both reduce the pressure computed in the shell volume.

Considering the bare silicon sphere, this small particle is under compression because of surface curvature (surface tension). This state remains during stage I, until a few 100 O atoms have been inserted. When the oxide layer becomes continuous (stage II), the volume expansion resulting from oxidation of the silicon is restrained by the silicon substrate. This is similar to the compressive stress resulting from epitaxial growth of a film with a lattice parameter larger than the substrate. The counterpart of the oxide compression is the tension obtained in the silicon core. The oxide shell that aims

Downloaded 02 Jul 2002 to 132.166.68.80. Redistribution subject to AIP license or copyright, see http://ojps.aip.org/japo/japcr.jsp

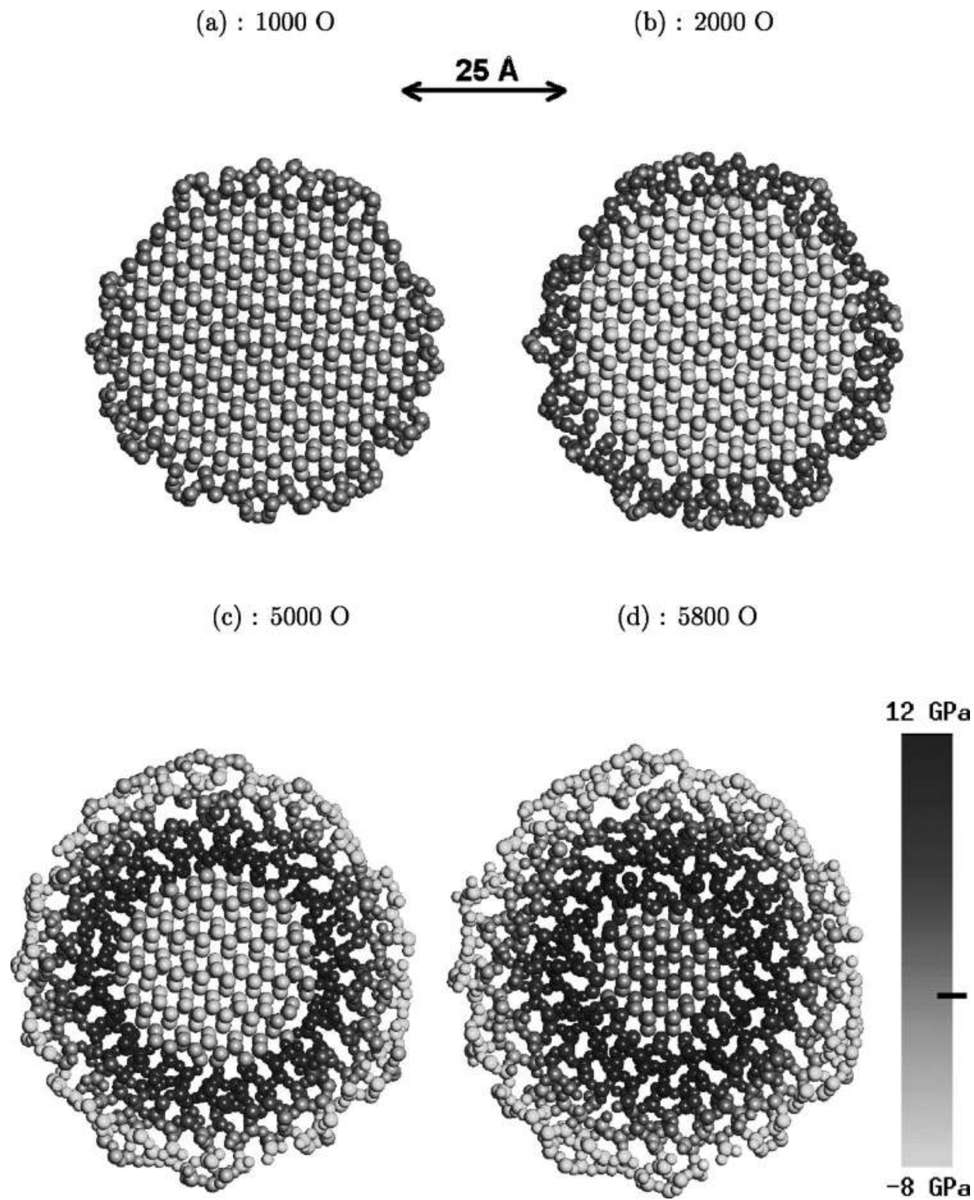

FIG. 7. (a) 6 Å thick sections from three-dimensional simulations of the oxidation of an initial 50 Å diam silicon sphere. Shown is the morphology after (a) 1000, (b) 2000, (c) 5000 and (d) 5800 oxygen atoms are inserted. The gray scale represents the pressure in the shells. The different structure between silicon (crystalline) and SiO_2 (disordered) and their different pressure state show the location of the Si/SiO_2 interface.

at expending, stretches the silicon core. As the oxide grows at the interface, it pushes out the old oxide, the external radius increases and the external shell is stretched (stage III). Finally, the oxide layer gets stiff and no longer accommodates volume expansion at the interface. The insertion of new oxygen pushes both sides of the interface. It produces an increase of interface pressure and changes the pressure in the silicon core from tensile to compressive.

As soon as a continuous oxide layer is formed, the stress tensor obtained in our simulations in the silicon is

$$\begin{pmatrix} \sigma & 0 & 0 \\ 0 & \sigma & 0 \\ 0 & 0 & \sigma \end{pmatrix}, \tag{8}$$

with $\sigma=\sigma_{rr}=\sigma_{\theta\theta}=\sigma_{\varphi\varphi}$, and in the oxide, the typical tensor is

$$\begin{pmatrix} \sigma_n & 0 & 0 \\ 0 & \sigma_t & 0 \\ 0 & 0 & \sigma_t \end{pmatrix}, \tag{9}$$

with $\sigma_n=\sigma_{rr}$ and $\sigma_t=\sigma_{\theta\theta}=\sigma_{\varphi\varphi}$.

Figure 8 shows the variation of the stress components σ_{rr}, $\sigma_{\theta\theta}$ and $\sigma_{\varphi\varphi}$ with the shell location at radius r. The stress components correspond to the morphology presented in Fig. 7(c) after 5000 oxygen insertions. Figure 8 shows the uniform isostatic pressure and the isotropic stress in the silicon (within the large fluctuations of the first data point). While σ_{rr} varies from tension to compression through the interface, the $\sigma_{\theta\theta}$ and $\sigma_{\varphi\varphi}$ plots indicate some discontinuity at the interface and a variation that is almost linear from compression at the interface to tension at the surface (the last data point corresponds again to a poorly filled volume). The

Downloaded 02 Jul 2002 to 132.166.68.80. Redistribution subject to AIP license or copyright, see http://ojps.aip.org/japo/japcr.jsp

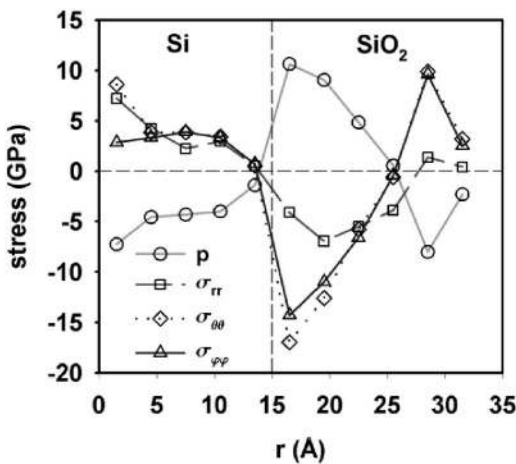

FIG. 8. Pressure (p) and normal (σ_{rr}) and tangential ($\sigma_{\theta\theta}$ and $\sigma_{\varphi\varphi}$) stress components as a function of the radial coordinate after 5000 oxygen atoms are inserted. The horizontal dashed line indicates zero stress while the vertical dashed line identifies Si/SiO_2 interface.

pressure shows similar behavior, i.e., a pressure gradient from compressive to tensile at the surface of the oxide shell.

Using classical continuum analysis of self-limiting oxidation it is concluded that the oxidation is slowed down by compressive stress in the silicon core.[1,11,12] We do observe compressive isotropic stress, but only beyond a given oxide thickness (15–20 Å in our modeling). For thin oxides, the computed stress is isotropic and tensile and should increase the growth rate according to phenomenological Eq. (2), which is at variance with the above mentioned argument.

Structural observations were carried out on oxidized spheres with silicon core diameters ranging from about 20 to 300 Å.[3] High resolution electron microscopy images were employed to measure the spacing of {111} plane fringes. Hofmeister and co-workers[3] observed either tensile or compressive stress in the silicon at self-limitation, depending on the silicon core diameter. These observations support our

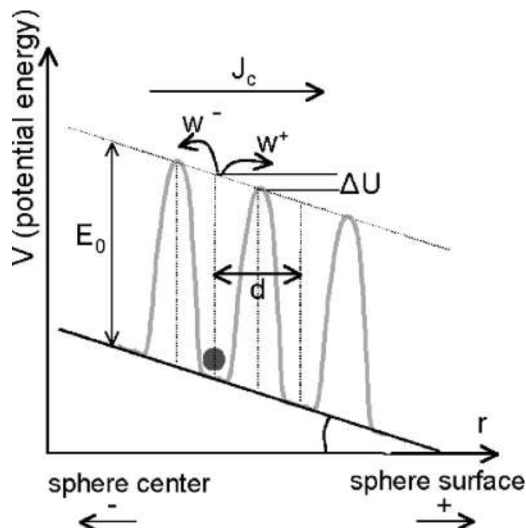

FIG. 9. Potential energy map of an O_2 molecule in SiO_2, where d is the jump distance in the r direction, E_0 is the diffusion barrier without a stress gradient, and w^+ and w^- are the jump rates along the oriented r-axis.

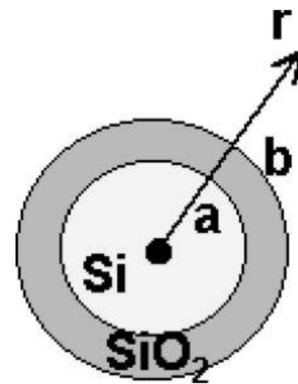

FIG. 10. Sketch of the silicon sphere in the oxide shell.

modeling with regard to isostatic tensile pressure being built up during oxidation and is not explained by classical arguments.

It was proposed by Liu *et al.*[5] that oxidant diffusion may play an important role in the limiting process. Transmission electron microscope micrographs were used to measure the self-limiting core diameter of silicon nanowires. The dependence of the limiting core diameter with oxide thickness favored the hypothesis of oxidant diffusion as a limiting mechanism. Delph[8] developed a continuum elastoviscoplastic model for cylinder oxidation that indicated the existence of a boundary layer near the Si/SiO_2 interface. This layer experiences large variations of $\sigma_{\theta\theta}$ and therefore of p. Our simulations do indeed indicate a pressure gradient in the oxide shell. It seems reasonable to believe that such stresses may affect oxidant transport.

V. OXIDANT TRANSPORT MODEL: APPLICATION TO DRY OXIDATION

Here we deal with a phenomenological description based on Nerst–Eintein's equation of transport through the oxide layer. Dry oxidation models usually consider that O_2 is the diffusing oxidant species but other mechanisms have been proposed (see, e.g., Ref. 29). Recently, Roma *et al.*[30] have shown that the oxygen diffusion in α-quartz at oxygen partial pressure larger than $\sim 10^{-4}$ bar (at 1000 K) was dominated by O_2 interstitial diffusion mechanisms. This result should be dependent on the SiO_2 structure, but the O_2 partial pressure is far beyond this limit under most oxidation processing conditions. We will consider O_2 diffusion mechanisms in the following.

Compressive pressure reduces the solubility of the O_2 molecule in SiO_2 as it raises the potential energy of the molecule in its interstitial site, whereas tensile pressure increases its solubility for the opposite reason. A schematic of the potential energy map of an oxygen molecule submitted to a pressure gradient along the radial direction (spherical coordinates) is presented in Fig. 9. The pressure gradient introduces bias into the diffusion process by lowering the barrier $(E_0 - \Delta U)$ toward the surface of the sphere by ΔU and increasing the barrier $(E_0 + \Delta U)$ toward the center of the sphere by the same amount, resulting in $w^+ > w^-$.

Downloaded 02 Jul 2002 to 132.166.68.80. Redistribution subject to AIP license or copyright, see http://ojps.aip.org/japo/japcr.jsp

This scheme can be formulated with in the framework of Nerst–Eintein theory that split transport in a diffusion term of the oxygen molecules with a convection term including a radial force induced by the pressure gradient. A convection flux $\mathbf{J_c}=c\mathbf{v}$ is added to Fick's flux expression:

$$\mathbf{J}=-D\nabla c+c\mathbf{v}=-D\nabla c+c\frac{Df_r}{k_BT}\mathbf{e_r}, \tag{10}$$

where $\mathbf{J}$ is the O_2 flux, D is the diffusion coefficient, c the O_2 concentration, $\mathbf{v}=v\mathbf{e_r}$ the drift velocity and $f_r\mathbf{e_r}$ a constant force on the O_2 molecules, directed in the radial $\mathbf{e_r}$ direction.

f_r is defined by

$$f_r=-\frac{\partial V}{\partial r}=-\nabla p v_{O_2}, \tag{11}$$

V is the potential energy of the O_2 molecule in the SiO_2 including the pressure effect, ∇p (scalar negative and constant) is the pressure gradient in the radial direction and v_{O_2} is the solubility volume of molecular O_2 in the SiO_2 network. The vibrational entropy changes are assumed to be negligible compared to the potential energy changes that result from the pressure gradient.

From Fig. 9, we assume that D is not affected by the pressure gradient. This is a simplified situation to provide a simple solution to the following transport equation. A more realistic description would involve the pressure and therefore spatial dependence of the diffusion coefficient. This is discussed further. Assuming that the O_2 concentration is only r dependent, the steady-state concentration $c(r)$ can be obtained by solving

$$\frac{\partial c}{\partial t}=-\mathrm{div}\,\mathbf{J}=D\Delta c-\mathbf{v}\nabla c=\frac{\partial^2 c}{\partial r^2}+\frac{\partial c}{\partial r}\left(\frac{2}{r}-\gamma\right)=0, \tag{12}$$

where, from relations (10) and (11),

$$\gamma=\frac{v}{D}=\frac{-\nabla p v_{O_2}}{k_BT}. \tag{13}$$

The solution is

$$c(r)=A\left(-\frac{\exp(\gamma r)}{r}+\gamma Ei(\gamma r)\right)+B, \tag{14}$$

where Ei is the exponential integral function defined by $Ei(x)=\int_{-\infty}^{x}[\exp(t)/t]dt$, $x>0$.

Coefficients A and B are determined from the boundary conditions at $r=a$ (the Si/SiO_2 interface in Fig. 10) and $r=b$ (the SiO_2 surface in Fig. 10) by applying the usual flux conditions,[9] i.e., the O_2 flux in the oxide at the Si/SiO_2 interface [Eq. (10)] balances the O_2 that is consumed to form SiO_2, K being the surface reaction rate constant:

$$J(a)=-Kc(a). \tag{15}$$

The O_2 flux at the SiO_2 surface is equal to the flux entering the oxide from the ambient:

$$J(b)=-h[c^*-c(b)]. \tag{16}$$

h is the surface mass transfer constant of the oxidant and c^* is the oxidant solubility at the surface and we account for its pressure dependence [Eq. (3)].

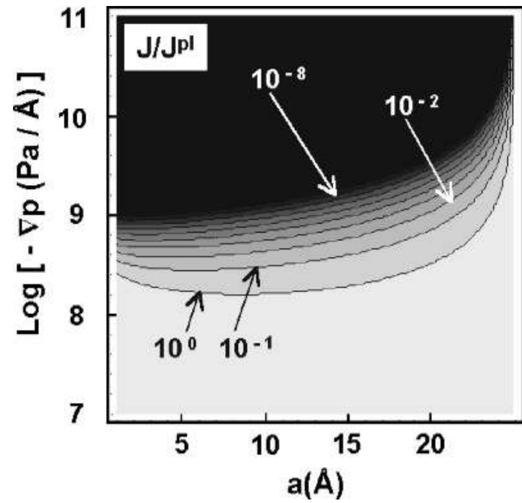

FIG. 11. Contour plot of the sphere to planar oxidation flux ratio J/J^{pl}. The contour lines indicate variations of this ratio by an order of magnitude. The gray scale corresponds to J/J^{pl} values (within the same order of magnitude). The lightest gray corresponds to $J/J^{pl}>1$ while the darkest corresponds to $J/J^{pl}<10^{-10}$.

We obtain

$$A=-\frac{\frac{h}{D}}{\gamma-\frac{h}{D}}c^*\left[\gamma Ei(\gamma b)-\gamma Ei(\gamma a)+\frac{\exp(\gamma a)}{a}\left(\frac{1}{a\left(\gamma+\frac{K}{D}\right)}+1\right)-\frac{\exp(\gamma b)}{b}\left(\frac{1}{b\left(\gamma-\frac{h}{D}\right)}+1\right)\right]^{-1}, \tag{17}$$

and

$$B=A\left[-\gamma Ei(\gamma a)+\frac{\exp(\gamma a)}{a}\left(\frac{1}{a\left(\gamma+\frac{K}{D}\right)}+1\right)\right]. \tag{18}$$

It is usual to consider that $h\gg K$, D/b and v (for the parameters and the pressure range of interest). We obtain, by combining Eqs. (14), (15), (17) and (18), the flux at the Si/SiO_2 interface:

$$J(a)=-K\frac{\exp(\gamma a)}{a^2\left(\gamma+\frac{K}{D}\right)}c^*\left[\gamma Ei(\gamma b)-\gamma Ei(\gamma a)+\frac{\exp(\gamma a)}{a}\left(\frac{1}{a\left(\gamma+\frac{K}{D}\right)}+1\right)-\frac{\exp(\gamma b)}{b}\right]^{-1}. \tag{19}$$

Downloaded 02 Jul 2002 to 132.166.68.80. Redistribution subject to AIP license or copyright, see http://ojps.aip.org/japo/japcr.jsp

By considering planar oxidation, the flux at the Si/SiO_2 interface of an oxide of identical thickness $\Delta z = b - a$ ($z = a$ corresponds to the Si/SiO_2 interface and $z = b$ corresponds to the SiO_2 surface) is given by[9]

$$J^{\text{pl}}(a) = -\frac{c^{*\text{pl}}}{\frac{1}{K^{\text{pl}}} + \frac{b-a}{D^{\text{pl}}}}. \tag{20}$$

The superscript pl stands for planar oxidation.

The self-limiting oxidation of spheres or cylinders is related to an oxide growth rate which is significantly reduced with respect to planar oxidation. We study the ratio between planar and sphere (with a pressure gradient) fluxes at the Si/SiO_2 interface $J(a)/J^{\text{pl}}(a) = F(a,b,c^*/c^{*\text{pl}},\nabla p, v_{O_2},T,K,D,K^{\text{pl}},D^{\text{pl}})$.

For the sake of tractability, we introduce further simplifications. We choose $D = D^{\text{pl}}$, neglecting again any stress dependence. Next, our goal is to estimate the effect of the pressure gradient on the oxidation kinetics. We neglect variations in the reaction rate constant, thus $K = K^{\text{pl}}$. We make use of the values of the kinetic parameters given by Liu *et al.*,[5] that are at $T = 1200$ K: $D \sim 8.3 \times 10^6$ Å^2/s and $K \sim 1.7 \times 10^4$ Å/s. The solubility volume v_{O_2} is an important parameter that appears in the expressions of γ [Eq. (13)] and of the solubility under pressure c^* [Eq. (3)]. We could not find any experimental or simulation data concerning v_{O_2}, but it may be estimated to ~20 Å^3 from the O_2 volume obtained by molecular theories.[7] $c^*/c^{*\text{pl}} = \exp\{-[p(b) - p^{\text{pl}}(b)]v_{O_2}/k_BT\}$ depends on the pressure at the SiO_2 surface which varies during oxidation. We know that the pressure obtained by molecular dynamics is overestimated. We can assume reasonable values (one order of magnitude lower) near the self-limiting regime and estimate $c^*/c^{*\text{pl}} \sim 6$ with $p^{\text{pl}}(b) \sim 0.5$ and $p(b) \sim -1$ GPa.

In MD, the initial radius of the silicon core was 25 Å and it was larger at the end of oxidation because of volume expansion ($v_{SiO_2} > v_{Si}$). In the analytical model this radius corresponds to b and varies during oxidation. We neglect this expansion and we set $b = 25$ Å in order to reduce the number of parameters. One might have considered the opposite point of view, i.e., a constant a and a variable b with similar discussions.

It is now convenient to plot $J(a)/J^{\text{pl}}(a)$ as a function of the remaining parameters a and ∇p in Fig. 11. The dark area corresponds to $J \ll J^{\text{pl}}$ by orders of magnitude. It corresponds to self-limitation, i.e., the oxide growth rate is more than 10^{10} slower than for planar oxidation. The extent of the dark area increases when a is smaller [it corresponds to a thicker ($b - a$) oxide] and/or when ($-\Delta p$) is larger (large f_r), which is intuitively appealing. The light gray area gives a range of parameters where sphere oxidation proceeds faster than planar oxidation. Singular behavior is observed at small a where the pressure gradient necessary to slow down the oxidation increases. In the absence of stress the larger the curvature, the faster the oxidation because of greater exposure to the ambient.[1] At small a, this effect acts against the pressure gradient.

A sharp transition between the two regimes ($J > J^{\text{pl}}$ and $J \ll J^{\text{pl}}$) appears for a wide range of a between $(-\Delta p) = 10^8$ and 10^9 Pa/Å. Self-limiting behavior should already be observable when the flux is at least 10 times slower than planar oxidation (contour line 10^{-1}). The pressure range is very sensitive to our choice of parameters, e.g., an increase of v_{O_2} by a factor of 2 would divide the limiting pressure gradients by the same factor. Note that these limiting pressure gradients are overestimated: the stress dependence of the diffusion coefficient that have been neglected in this work should further reduce the oxygen flux in the compressive regions [Eq. (2)] of the oxide near the Si/SiO_2 interface. In addition, 10^9 Pa/Å corresponds to the pressure gradients obtained in the MD simulations. We know that they may be overestimated, but experimentally, large strains (compressive and tensile >1%) are observed in the silicon core of nanospheres.[3] Such strain induces GPa pressures in the silicon. We would therefore expect comparable pressures in the oxide over thicknesses on the order a few 10 Å. This would correspond to pressure gradients ($-\Delta p \sim 10^8$ Pa/Å) comparable to the limiting pressure gradients in our model.

VI. SUMMARY AND CONCLUSIONS

Molecular dynamics simulations were performed to assess the oxidation energetics and kinetics of silicon nanospheres. The formation of silicon oxide from the silicon lattice was achieved by inserting atomic oxygen into the Si–Si bonds in an atom-by-atom way (thus, it does not assess the specific mechanisms and defects of the oxidation by particular species: O_2, H_2O or O).

We applied our model to field planar oxidation to test its capabilities. We found that the model provides qualitative agreement even if it overestimates the pressure in the oxide layer.

We then applied the simulation technique to the oxidation of 50 Å diam silicon nanospheres. We verified that stress built into the system cannot cause the oxidation reaction to stop for energetic considerations. We explored possible kinetic limitations by studying local stress in the system. We found the following.

For thin oxides, our model predicts tensile pressure in the silicon core and a pressure gradient in the SiO_2 from compressive at the interface to tensile at the surface. This is in contrast to continuum models. The tensile pressure in the silicon core was also reported in independent experiments.

For thicker oxides, we found compressive pressure in the silicon core just like that in continuum models but a large pressure gradient in the oxide.

Self-limitation is usually explained by a reduced oxidation reaction rate that results from isotropic compressive stress in the silicon core. However, self-limitation was also observed when the silicon core was under small compression or even under tension, thereby opening discussions of other hypotheses.

We studied the effect of the pressure gradient on O_2 transport during dry oxidation within the framework of Nerst–Einstein's transport theory. We found that self-limitation in the sense of a sharp drop in the oxidation rate is

Downloaded 02 Jul 2002 to 132.166.68.80. Redistribution subject to AIP license or copyright, see http://ojps.aip.org/japo/japcr.jsp

expected for pressure gradient values that are compatible with our simulations and with values estimated from experimental studies of atomic spacing in oxidized silicon nanospheres.

ACKNOWLEDGMENTS

One of the authors (J.D.T.) would like to acknowledge LETI/DTS for financial support and G. Roma, A. Estève, M. Djafari Rouhani, D. Estève, F. de Creçy and P. Donnadieu for fruitful discussions.

[1] D.-B. Kao, J. McVitte, W. Nix, and K. Saraswat, IEEE Trans. Electron Devices **ED-35**, 25 (1988).
[2] R. Okada and S. Iijima, Appl. Phys. Lett. **58**, 1662 (1991).
[3] H. Hofmeister, F. Huisken, and B. Kohn, Eur. Phys. J. D **9**, 137 (1999).
[4] H. Liu, D. Biegelsen, N. Johnson, F. Ponce, and R. Pease, J. Vac. Sci. Technol. B **11**, 2532 (1993).
[5] H. Liu, D. Biegelsen, F. Ponce, N. Johnson, and R. Pease, Appl. Phys. Lett. **64**, 1383 (1994).
[6] S. Tiwari, F. Rana, K. Chan, L. Shi, and H. Hanafi, Appl. Phys. Lett. **69**, 1232 (1996).
[7] C. Rafferty and R. Dutton, Appl. Phys. Lett. **54**, 1815 (1989).
[8] T. Delph, J. Appl. Phys. **83**, 786 (1998).
[9] B. Deal and A. Grove, J. Appl. Phys. **36**, 3770 (1965).
[10] C. Rafferty, Ph.D. thesis, Stanford University, Stanford, CA, 1989.
[11] Y. Chen, Proceedings of the Third International Conference on Modeling and Simulation of Microsystems, 2000, p. 56.
[12] Y. Chen and Y. Chen, Microelectron. Eng. **57–58**, 897 (2001).
[13] *Fundamental Aspects of Silicon Oxidation*, edited by Y. Chabal (Springer, New York, 2001).
[14] A. Estève, Y. Chabal, K. Raghavachari, M. Weldon, K. Queeney, and M. Djafari Rouhani, J. Appl. Phys. **90**, 6000 (2001).
[15] A. Estève, Ph.D. thesis, Université Paul Sabatier, Toulouse, France, 2000.
[16] J. Dalla Torre, M. Djafari Rouhani, R. Malek, D. Estève, and G. Landa, J. Appl. Phys. **84**, 5487 (1998).
[17] Y. Tu and J. Tersoff, Phys. Rev. Lett. **84**, 4393 (2000).
[18] K.-O. Ng and D. Vanderbilt, Phys. Rev. B **59**, 10 132 (1999).
[19] T. Watanabe and I. Ohdomari, Thin Solid Films **343–344**, 370 (1999).
[20] T. Watanabe, H. Fujiwara, H. Noguchi, T. Hoshino, and I. Ohdomari, Jpn. J. Appl. Phys., Part 2 **38**, L366 (1999).
[21] A. Stoneham, M. Szymanski, and A. Shluger, Phys. Rev. B **63**, 241304 (2001).
[22] E. Kodeba and E. Irene, J. Vac. Sci. Technol. B **5**, 15 (1987).
[23] J. Broughton, G. Gilmer, and J. Weeks, J. Chem. Phys. **75**, 5128 (1981).
[24] V. Vitek and T. Egami, Phys. Status Solidi B **144**, 145 (1987).
[25] O. Nielsen and R. Martin, Phys. Rev. B **32**, 3780 (1985).
[26] E. Kodeba and E. Irene, J. Vac. Sci. Technol. B **4**, 720 (1986).
[27] E. EerNisse, Appl. Phys. Lett. **35**, 8 (1979).
[28] J.-P. Crocombette (unpublished results).
[29] D. Hamann, Phys. Rev. Lett. **81**, 3447 (1998).
[30] G. Roma, Y. Limoge, and S. Baroni, Phys. Rev. Lett. **86**, 4564 (2001).

Downloaded 02 Jul 2002 to 132.166.68.80. Redistribution subject to AIP license or copyright, see http://ojps.aip.org/japo/japcr.jsp